

Reengineering Ponatinib to Minimize Cardiovascular Toxicity



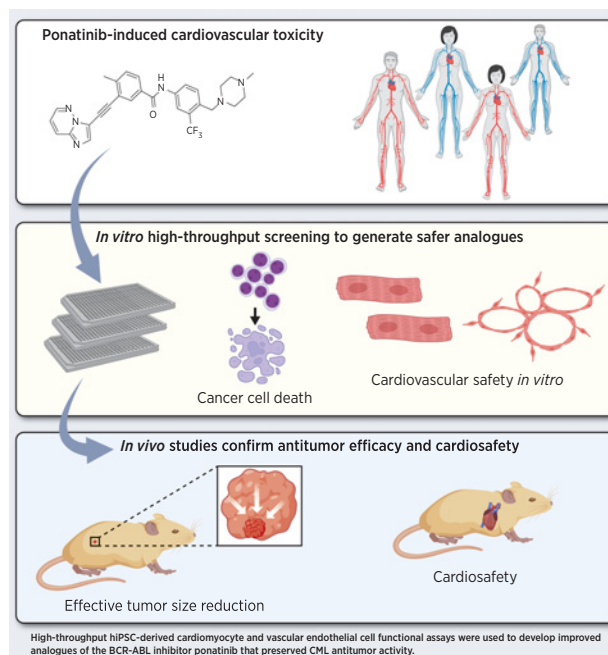
Anna P. Hnatiuk¹, Arne A.N. Bruyneel¹, Dhanir Tailor², Mallesh Pandrala², Arpit Dheeraj², Wenqi Li², Ricardo Serrano¹, Dries A.M. Feyen¹, Michelle M. Vu¹, Prashila Amatya¹, Saloni Gupta², Yusuke Nakauchi³, Isabel Morgado¹, Volker Wiebking⁴, Ronglih Liao¹, Matthew H. Porteus⁴, Ravindra Majeti³, Sanjay V. Malhotra², and Mark Mercola¹

ABSTRACT

Small molecule tyrosine kinase inhibitors (TKI) have revolutionized cancer treatment and greatly improved patient survival. However, life-threatening cardiotoxicity of many TKIs has become a major concern. Ponatinib (ICLUSIG) was developed as an inhibitor of the *BCR-ABL* oncogene and is among the most cardiotoxic of TKIs. Consequently, use of ponatinib is restricted to the treatment of tumors carrying T315I-mutated *BCR-ABL*, which occurs in chronic myeloid leukemia (CML) and confers resistance to first- and second-generation inhibitors such as imatinib and nilotinib. Through parallel screening of cardiovascular toxicity and antitumor efficacy assays, we engineered safer analogs of ponatinib that retained potency against T315I *BCR-ABL* kinase activity and suppressed T315I mutant CML tumor growth. The new compounds were substantially less toxic in human cardiac vasculogenesis and cardiomyocyte contractility assays *in vitro*. The compounds showed a larger therapeutic window *in vivo*, leading to regression of human T315I mutant CML xenografts without cardiotoxicity. Comparison of the kinase inhibition profiles of ponatinib and the new compounds suggested that ponatinib cardiotoxicity is mediated by a few kinases, some of which were previously unassociated with cardiovascular disease. Overall, the study develops an approach using complex phenotypic assays to reduce the high risk of cardiovascular toxicity that is prevalent among small molecule oncology therapeutics.

Significance: Newly developed ponatinib analogs retain antitumor efficacy but elicit significantly decreased cardiotoxicity,

representing a therapeutic opportunity for safer CML treatment.



¹Stanford Cardiovascular Institute and Department of Medicine, Stanford University, Stanford, California. ²Center for Experimental Therapeutics, Knight Cancer Institute, Oregon Health Sciences University School of Medicine, Portland, Oregon. ³Division of Hematology Institute for Stem Cell Biology and Regenerative Medicine, Stanford School of Medicine, California. ⁴Department of Pediatrics, Stanford School of Medicine, Stanford, California.

A.P. Hnatiuk, A.A.N. Bruyneel, D. Tailor, and M. Pandrala contributed equally to this article.

Corresponding Authors: Mark Mercola, Stanford Cardiovascular Institute, Biomedical Innovation Building, room 3300, 240 Pasteur Drive, Palo Alto, CA 94304. Phone: 650-721-3281; E-mail: mmercola@stanford.edu; and Sanjay V. Malhotra, 2720 S. Moody Ave, KCRB 2126; Portland, OR 97201. Phone: 971-712-4458; E-mail: malhotsa@ohsu.edu

Cancer Res 2022;82:2777-91

doi: 10.1158/0008-5472.CAN-21-3652

This open access article is distributed under the Creative Commons Attribution-NonCommercial-NoDerivatives 4.0 International (CC BY-NC-ND 4.0) license.

©2022 The Authors; Published by the American Association for Cancer Research

Introduction

The development of small molecule kinase inhibitor (KI) drugs over the last two decades has contributed to the substantial decline in death rates and improved survival of patients with cancer (1, 2). Currently, there are 52 small molecule tyrosine KIs (TKI) that have been approved by the FDA (3). However, as of early 2020, 73% of approved KIs were associated with treatment-related cardiotoxicity (4). Therefore, while TKIs have improved outcomes, they also cause chronic and potentially lethal cardiovascular side effects.

Chronic myeloid leukemia (CML) is a form of leukemia characterized by the Philadelphia (Ph) chromosome, which results from the *t(9;22)(q34;q11)* balanced reciprocal translocation (5), resulting in the *in vivo* created oncologic driver kinase *BCR-ABL*, supporting unhindered growth, survival, and proliferation (6, 7). After regulatory approval of the first-generation *BCR-ABL* inhibitor, imatinib mesylate, 5-year overall survival of CML increased up to 90% (8). Unfortunately, approximately 33% of patients with CML either do not respond or develop resistance to imatinib (9). Second-generation *BCR-ABL* inhibitors such as nilotinib and dasatinib were developed to mitigate resistance, however in 20% of resistant

cases, a kinase domain mutation replaces the threonine₃₁₅ (Thr₃₁₅) with a bulkier isoleucine that hinders entry of all approved BCR-ABL inhibitors except for the third-generation inhibitor ponatinib (ICLUSIG; refs. 10–14). Because of high incidence of serious and fatal cardiovascular events, such as vascular thrombotic events and development of heart failure, ponatinib was temporarily suspended from the market. Ponatinib is the only active site, first-line therapeutic with efficacy against tumors harboring the T315I “gate-keeper” mutation and its use is now restricted primarily to CML or Ph⁺ acute lymphoblastic leukemia (Ph⁺ALL) harboring T315I mutant BCR-ABL (15, 16).

In this study, we describe engineered analogues of ponatinib that retain antitumor efficacy yet have substantially reduced cardiotoxicity. Since the molecular targets of ponatinib that mediate its cardiotoxicity were unknown, we resorted to phenotypic assays of vasculogenesis, cardiomyopathy, and tumor cell growth inhibition to guide the medicinal chemistry optimization of ponatinib. Two refined analogues, 33a and 36a, showed efficacy against human T315I mutant CML xenografts with substantially decreased *in vivo* cardiotoxicity. To our knowledge, these compounds represent the first example of using phenotypic cardiotoxicity assays to decrease the cardiotoxicity liability of an oncology drug.

Materials and Methods

Chemistry methods: syntheses of 33a and 36a

All the reagents and solvents were obtained at the highest commercial quality from sources such as Sigma-Aldrich, Thermo Fisher Scientific, TCI International, etc. Flash chromatography was carried out using a CombiFlash Rf+ Lumen chromatography system (Teledyne ISCO). ¹H (400 MHz) and ¹³C (101 MHz) nuclear magnetic resonance (NMR) spectra were recorded on an Agilent 400-MR NMR, using appropriate deuterated solvents, as needed. Chemical shifts (δ) were reported in parts per million (ppm) upfield from tetramethylsilane (TMS) as an internal standard. LC/MS spectra were recorded on an Agilent 6490 iFunnel Triple Quadrupole Mass Spectrometer from Agilent Technologies Inc.

Procedure for the synthesis of inhibitor 36a (Supplementary Fig. S1A)

3-Iodo-4-methyl-N-(3-(4-methyl-1H-imidazol-1-yl)-5-(trifluoromethyl)phenyl)benzamide S-III

Under a nitrogen atmosphere, 3-Iodo-4-methylbenzoic acid S-II (2.5 g, 9.5 mmol) was taken in SOCl₂ (3.2 mL, 44.1 mmol) and then a drop of N, N-Dimethylformamide (DMF) was added at room temperature. The reaction mixture was stirred at reflux for 5 hours before it was cooled to room temperature and the excess SOCl₂ was carefully removed. The crude material was coevaporated with benzene and dried under vacuum to afford the desired acid chloride. The acid chloride was dissolved in anhydrous THF (10 mL) and then added dropwise to a stirred mixture of 3-(4-Methyl-1H-imidazol-1-yl)-5-(trifluoromethyl)aniline S-I (2.0 g, 8.3 mmol), diisopropylethylamine (1.98 mL, 11.4 mmol), and 4-Dimethylaminopyridine (DMAP; 0.12 g, 0.98 mmol) in THF at 0°C. Upon completion of the addition, the reaction mixture was warmed to room temperature and stirred overnight. The reaction was quenched with water, and the product was extracted into ethyl acetate (3 × 30 mL). The combined organic extracts were washed with brine solution (25 mL), dried over Na₂SO₄, filtered, and evaporated to dryness to afford a crude material that was purified on a silica gel column using a 0% to 50% gradient of ethyl

acetate in hexane as eluent to obtain the desired product as an off-white solid (3.83 g, 95% yield). ¹H NMR (400 MHz, DMSO-*d*₆) δ 10.68 (s, 1H), 8.45 (s, 1H), 8.27 (s, 1H), 8.20 (s, 1H), 8.13 (s, 1H), 7.93 (d, *J* = 8.0 Hz, 1H), 7.72 (s, 1H), 7.55–7.40 (m, 2H), 2.44 (s, 3H), 2.18 (d, *J* = 2.4 Hz, 3H). ¹³C NMR (101 MHz, DMSO-*d*₆) δ 164.58, 145.82, 141.61, 139.39, 138.36, 137.94, 135.41, 133.60, 131.45, 130.34, 128.32, 125.46, 122.75, 115.39, 114.64, 112.15, 101.63, 28.05, 14.03. LC/MS (ESI-QQQ): *m/z* 486.00 [(C₁₉H₁₅F₃IN₃O + H)⁺ calculated 486.02]. Purity: 97.5% [retention time (*t*_R) = 4.773 minutes].

3-(Imidazo[1,2-*b*]pyridazin-3-ylethynyl)-4-methyl-N-(3-(4-methyl-1H-imidazol-1-yl)-5-(trifluoromethyl)phenyl)benzamide 36a

The title compound was prepared according to the previously reported methods for similar with several modifications (17). 3-Iodo-4-methyl-N-(3-(4-methyl-1H-imidazol-1-yl)-5-(trifluoromethyl)phenyl)benzamide (0.2 g, 0.41 mmol) was added to a stirred solution of 3-Ethynylimidazo[1,2-*b*]pyridazine S-IV (0.06 g, 0.41 mmol) in DMF (10 mL). The mixture underwent three cycles of vacuum/filling with nitrogen and then CuI (0.007 g, 0.04 mmol), Pd(PPh₃)₄ (0.05 g, 0.04 mmol), and diisopropylethylamine (0.14 mL, 0.82 mmol) were added. The reaction mixture was stirred at 80°C for 2 hours before it was cooled to room temperature. Water (25 mL) was added and the product extracted into ethyl acetate (3 × 25 mL). The organic layers were combined, washed with water (20 mL), 0.5N NH₄OH solution (10 mL), followed by brine solution (20 mL). The organic phase was dried over Na₂SO₄, filtered, and then evaporated to dryness to afford crude product, which was then triturated with diethyl ether to yield a solid. The solid was collected by filtration, washed with copious amounts of ether and dried under vacuum to furnish the desired compound as a pale-yellow solid (160 mg, 77% yield). ¹H NMR (400 MHz, DMSO-*d*₆) δ 10.72 (s, 1H), 8.71 (d, *J* = 4.4 Hz, 1H), 8.39 – 8.06 (m, 6H), 7.99 – 7.89 (m, 1H), 7.72 (s, 1H), 7.56 (d, *J* = 8.1 Hz, 1H), 7.48 (s, 1H), 7.38 (dd, *J* = 9.3, 4.4 Hz, 1H), 2.60 (s, 3H), 2.16 (s, 3H). ¹³C NMR (101 MHz, DMSO-*d*₆) δ 165.29, 145.53, 144.31, 141.66, 140.21, 140.12, 139.42, 138.74, 138.39, 135.52, 132.30, 131.3, 130.68, 130.58, 129.00, 126.57, 124.1, 122.32, 119.57, 115.43, 114.81, 112.15, 110.00, 96.77, 81.71, 20.88, 14.02. LC/MS (ESI-QQQ): *m/z* 501.30 [(C₂₇H₁₉F₃N₆O + H)⁺ calculated 501.16]. Purity: 99% (*t*_R = 4.427 minutes).

Procedure for the synthesis of inhibitor 33a (Supplementary Fig. S1B)

N-(3-Bromo-5-(trifluoromethyl)phenyl)-3-iodo-4-methylbenzamide S-VI

Under a nitrogen atmosphere, 3-Iodo-4-methylbenzoic acid S-II (5.0 g, 19.08 mmol) was taken in SOCl₂ (6.5 mL, 89.6 mmol) and then two drops of DMF were added at room temperature. The reaction mixture was stirred at reflux for 5 hours before it was cooled to room temperature and the excess SOCl₂ was carefully removed. The crude material was coevaporated with benzene and dried under vacuum to afford the desired acid chloride. The acid chloride was dissolved in anhydrous THF (20 mL) and then added dropwise to a stirred mixture of 3-bromo-5-(trifluoromethyl)aniline S-V (4.57 g, 19.08 mmol), diisopropylethylamine (3.97 mL, 22.8 mmol), and DMAP (0.23 g, 1.88 mmol) in THF at 0°C. Upon completion of the addition, the reaction mixture was warmed to room temperature and stirred overnight. The reaction was quenched with water, and the product was extracted into ethyl acetate (3 × 50 mL). The combined organic extracts were washed with brine solution (25 mL), dried over Na₂SO₄, filtered, and evaporated to dryness to afford a crude material that was

purified on a silica gel column using a 0% to 50% gradient of ethyl acetate in hexane as eluent to obtain the desired product as an off-white solid (7.6 g, 82% yield). ¹H NMR (400 MHz, DMSO-*d*₆) δ 10.61 (s, 1H), 8.49–8.29 (m, 2H), 8.19 (s, 1H), 7.91 (dd, *J* = 7.9, 1.9 Hz, 1H), 7.67 (s, 1H), 7.50 (d, *J* = 7.9 Hz, 1H), 2.44 (s, 3H). ¹³C NMR (101 MHz, DMSO-*d*₆) δ 164.63, 145.89, 141.74, 137.94, 133.53, 131.73, 130.35, 128.34, 126.48, 124.98, 123.04, 122.67, 115.92, 101.63, 28.06. LC/MS (ESI-QQQ): *m/z* 483.90 [(C₁₅H₁₀BrF₃INO + H)⁺ calculated 483.89]. Purity: 99% (*t*_R = 6.410 minutes).

N-(3-Bromo-5-(trifluoromethyl)phenyl)-3-(imidazo[1,2-b]pyridazin-3-ylethynyl)-4-methylbenzamide S-VII

This was prepared using N-(3-Bromo-5-(trifluoromethyl)phenyl)-3-iodo-4-methylbenzamide S-VI (2.0 g, 4.13 mmol) and 3-Ethynylimidazo[1,2-b]pyridazine S-IV (0.62 g, 4.33 mmol) as shown in Supplementary Fig. S1B using a similar method that was described for the synthesis of 33a. The desired product was obtained as an off-white solid (1.42 g, 69% yield). ¹H NMR (400 MHz, DMSO-*d*₆) δ 10.69 (s, 1H), 8.72 (dd, *J* = 4.4, 1.5 Hz, 1H), 8.39 (t, *J* = 1.9 Hz, 1H), 8.31–8.17 (m, 3H), 7.94 (dd, *J* = 8.0, 2.0 Hz, 1H), 7.69–7.52 (m, 3H), 7.39 (dd, *J* = 9.2, 4.4 Hz, 1H), 2.61 (s, 3H). ¹³C NMR (101 MHz, DMSO-*d*₆) δ 165.32, 145.51, 144.31, 141.81, 138.74, 132.20, 131.98, 131.88, 131.71, 131.39, 130.63, 129.26, 129.14, 128.99, 126.56, 126.44, 122.66, 122.31, 119.54, 115.85, 96.76, 81.70, 20.87. LC/MS (ESI-QQQ): *m/z* 499.1 [(C₂₃H₁₄BrF₃N₄O + H)⁺ calculated 499.03]. Purity: 95.8% (*t*_R = 6.040 minutes).

N-(3-(1H-Imidazol-1-yl)-5-(trifluoromethyl)phenyl)-3-(imidazo[1,2-b]pyridazin-3-ylethynyl)-4-methylbenzamide 33a

Compound 33a was prepared according to the previously reported methods for similar compounds (18, 19), with several modifications. N-(3-Bromo-5-(trifluoromethyl)phenyl)-3-[imidazo(1,2-b)pyridazin-3-ylethynyl]-4-methylbenzamide S-VII (3.0 g, 6.00 mmol) and 1H-Imidazole (0.45 g, 6.61 mmol) were taken in dry DMSO (50 mL) in a pressure tube. The solution was purged with a nitrogen flow for 10 minutes then CuI (0.17 g, 0.90 mmol), K₂CO₃ (2.5 g, 18.0 mmol), and 8-hydroxyquinoline (0.13 g, 0.90 mmol) were added and purging was continued for another 10 minutes. The pressure tube was then sealed tightly and stirred at 100°C for 18 hours. Upon cooling to room temperature, the reaction mixture was poured into ice-cold water (~50 mL) and allowed to stir for 30 minutes, during which time pale yellow solid was observed. The solid was collected by filtration and then dissolved in 10% MeOH in dichloromethane (100 mL). The undissolved solid was removed by filtration. The filtrate was evaporated to dryness to afford crude product, which was purified on a silica gel column using a 0% to 10% gradient of methanol in dichloromethane as an eluent to obtain the desired product as a pale-yellow solid (1.67 g, 57% yield). ¹H NMR (400 MHz, DMSO-*d*₆) δ 10.78 (s, 1H), 8.73 (dt, *J* = 4.5, 1.4 Hz, 1H), 8.34 (s, 2H), 8.30–8.19 (m, 4H), 7.98 (dd, *J* = 8.1, 1.9 Hz, 1H), 7.81 (d, *J* = 9.6 Hz, 2H), 7.59 (d, *J* = 8.1 Hz, 1H), 7.40 (ddd, *J* = 9.2, 4.5, 1.1 Hz, 1H), 7.18 (s, 1H), 2.63 (s, 3H). ¹³C NMR (101 MHz, DMSO-*d*₆) δ 165.32, 145.54, 144.33, 141.68, 140.2, 138.75, 138.5, 132.29, 131.32, 130.91, 130.70, 130.59, 129.02, 126.58, 124.1, 122.33, 119.58, 116.04, 115.20, 112.78, 112.71, 112.19, 100.30, 96.77, 81.72, 20.89. LC-MS (ESI-QQQ): *m/z* 487.20 [(C₂₆H₁₇F₃N₆O + H)⁺ calculated 487.14]. Purity: 99% (*t*_R = 4.510 minutes).

K562 cell culture and K562-T315I derivation

The K562-wildtype (WT) cells (CCL-243 ATCC) were cultured in suspension in RPMI 1640 (Gibco #11875119, Thermo Fisher Scientific) supplemented with 10% FBS (Gibco #26140079, Thermo Fisher

Scientific), and 1% Pen/Strep/L-Glutamine (Gibco #25030081, Thermo Fisher Scientific) at 37°C and 5% CO₂. The BCR-ABL T315I mutant CML model was generated by introducing the “gate-keeper” BCR-ABL T315I mutation using CRISPR/Cas9 gene editing of K562-WT cells (Supplementary Fig. S2A). One million K562-WT cells were seeded in six-well plates and transfected with Lipofectamine 2000 (Invitrogen #11668019, Thermo Fisher Scientific) and 1 μg of CRISPR/Cas9 vector (pSpCas9(BB)-2A-GFP; Addgene #48138) incorporating the guide sequence (CTCAGTGATGATATAGAACG), and Lipofectamine RNAiMax (Invitrogen #13778500, Thermo Fisher Scientific) and 4 μg of ssDNA donors (1 μg of each donor): [homology-directed repair (HDR) template1: CGTGTGAAGTCCTCGTTGTCTTGTGGCAGGGGTCTGCACCCGGGAGCCCCGTTCTATATCATCATTTGAGTTCATGACCGGAACTCTGGACT; HDR template2: TTCAGTTGAGCGGAGCCACCTGTTGAAGTCCCTCGTTGTCTTGTGGCAGGGGTCTGCACCCGGGAGCCCCGTTCTATATCATCATTTGAGTTCATGAC; HDR template3: CGTGTGAAGTTCCTCGTTGTCTT-GTTGGCAGGGGTCTGCACCCGGGAGCCACCGTTCTATATCATCATTTGAGTTCATGACCTACGGAACCTCTGGACT; and HDR template4: TTCAGTTGGGAGCGGAGCCACCTGTTGAAGTTCCTCGTTGTCTTGTGGCAGTTTCATGAC] for each well of a six-well plate. The cells were left to recover and proliferate, before being selected using 1 μmol/L of imatinib in RPMI supplemented with 10% FBS. After establishing an enriched polyclonal pool of drug-resistant K562 cells, imatinib selection was stopped, and the cells were cultured in RPMI supplemented with 10% FBS. Sanger sequencing revealed the presence of the T315I mutation in both DNA and RNA in the imatinib-resistant K562 clones, but not K562-WT clones. To determine drug resistance, the cells were treated for 48 hours with a panel of KIs (imatinib, nilotinib, dasatinib, bosutinib, asciminib, ponatinib, rebastinib, tozasertib; Tocris Bioscience, Selleckchem). The K562-WT cell line was susceptible to all compounds, whereas the K562-T315I cell line was resistant to all compounds except for ponatinib, tozasertib, asciminib, and rebastinib (Supplementary Fig. S2B). Sensitivity to asciminib could be restored by treatment with cyclosporine A (10 μmol/L), suggesting that asciminib, like imatinib, is sensitive to ABCB1-mediated efflux (Supplementary Fig. S2C) as reported (20).

KCL22-WT and KCL22-T315I cell culture

The KCL22-WT and KCL22-T315I cells that were a gift from Dr. Robert A. Kirken and Dr. Georgialina Rodriguez (21) were cultured in suspension in RPMI 1640 (Gibco #11875119, Thermo Fisher Scientific) supplemented with 10% FBS (Gibco #26140079, Thermo Fisher Scientific), and 1% Pen/Strep +2 mmol/L L-Glutamine (Gibco #25030081, Thermo Fisher Scientific).

BaF3-WT and BaF3-T315I cell culture

The BaF3-WT and BaF3-T315I cell lines (22) that were a gift from Dr. Brian Druker were cultured in RPMI 1640 (Gibco #11875119, Thermo Fisher Scientific) supplemented with 10% FBS (Gibco #26140079, Thermo Fisher Scientific) and 1% Pen/Strep (Gibco #25030081, Thermo Fisher Scientific).

Human cardiac microvascular endothelial cells culture

The human cardiac microvascular endothelial cells (HMVEC-C) were purchased from Lonza (Lonza #CC-7030, batch 0000550176), primary cell prevent from healthy male donor, age 55 years old. HMVEC-Cs were seeded on 0.1% gelatin in water (STEMCELL Technologies # 07903) precoated Nunc EasYFlask 75 cm² and

175 cm² flasks (Thermo Fisher Scientific #159910) and cultured in EBMTM-2 Basal Medium (Lonza #CC-3156) and EGMTM-2 MV supplemented with microvascular endothelial cell growth medium SingleQuots™ (Lonza #CC-4147). HMVEC-Cs were expanded and used between passages 6 and 7 to perform the vasculogenesis assay. Each cell expansion was considered as a different biological batch.

Human-induced pluripotent stem cells cell culture and differentiation to cardiomyocytes

The human-induced pluripotent stem cells (hiPSC) and protocols were approved by the Stanford University (Stanford, CA) Institutional Review Board and Stem Cell Research Oversight committees. This study used preexisting hiPSC lines that were generated with informed written consent by each donor. The hiPSC lines were from 2 healthy donors with no history of cardiovascular disease from the Stanford Cardiovascular Institute Biobank: hiPSCs HD.15S1 (male), and hiPSCs HD.273 (female). All hiPSC lines had been reprogrammed using nonintegrating Sendai viral vectors. Methods to ensure the identity and validity of the hiPSCs include SNP karyotyping using Illumina's CytoSNP-850K genotyping microarrays, physiological verification of contractile function, and regular *Mycoplasma* testing using MycoAlert Mycoplasma Detection Kit (Lonza, LT07-318). The hiPSC clones were cultured in E8 cell culture media (Gibco, #A1517001, Thermo Fisher Scientific) in plates coated with Geltrex-LDEV-Free Reduced Growth Factor Basement Membrane Matrix (Gibco #A1413202, Thermo Fisher Scientific) until at least passage 20 before differentiation. Once confluent, the hiPSCs were differentiated into human cardiomyocytes (CM) utilizing a differentiation and maturation protocol as described (23). Briefly, differentiation was initiated by treatment with CHIR99021 (Tocris #4423) for 3 days in RPMI 1640 with B27 minus insulin (Gibco #A1895601, Thermo Fisher Scientific). Subsequently the cells were treated with the Wnt inhibitor C59 (Tocris #5148) in RPMI/B27 minus insulin for another 2 days. Between 6 to 9 days of differentiation, RPMI/B27 minus insulin was used and changed every other day and switched to RPMI/B27 plus insulin at day 10 of differentiation after beating was observed for 2 days. To improve the CM purity, cells were cultured in RPMI/B27 plus insulin without glucose for 3 days and then switched for RPMI/B27 plus insulin for 1 day. On day 15, the hiPSC-CMs were dissociated with TrypLE 10x (Gibco #A1217703, Thermo Fisher Scientific) and seeded in six-well Geltrex coated plates at 3×10^6 hiPSC-CMs per well in RPMI/B27 plus insulin containing 10% knockout serum replacement (KOSR; Gibco #10828028, Thermo Fisher Scientific) and ROCK inhibitor Y-27632 (Tocris #1253; replating medium). At day 30 of differentiation the cells were exposed to a fatty acid rich maturation medium (MM; ref. 23) and cultured for at least 5 weeks in MM prior to replating in 384-well plates (Greiner µClear #781090, Greiner Bio-One) for high-throughput screening.

Phenotypic screening of antiproliferative activity in human CML cell lines K562 and KCL22

CML cell proliferation *in vitro* was evaluated by the AlamarBlue assay using the NCI 60 human tumor cell line anticancer drug screen (NCI60) methodology that yielded growth inhibition 50% (GI₅₀) values as a quantitative measure of viability (24). Three different batches of cells/line were harvested and plated in 384-well plates (Greiner µClear) at 1,300 cells per well and incubated for 24 hours at 37°C. The next day, all the compounds were screened in at three-fold dilution series, with four technical replicates and incubated for 48 hours

at 37°C. Maximum doses of ponatinib, 33a, 36a, and nilotinib were 10 µmol/L for the K562 cell line and 1.11 µmol/L for the KCL22 cell line. At this point, the cells were treated with Resazurin (final concentration 10%; R&D Systems #AR002) and incubated for 2 hours before measuring fluorescence on a plate reader (excitation 544 nm, emission 590 nm) to quantify the antiproliferative effects of the compounds.

Phenotypic screening of antiproliferative activity in murine cell line BaF3

CML cell proliferation was evaluated by CellTiter-Glo 3D cell viability assay (Promega #G9681). Cells were harvested and plated in white 96-well plates (Falcon #353296) at 3,000 cells per well and incubated for 24 hours at 37°C. The next day, all the compounds were screened in at three-fold dilution series, with three technical replicates and incubated for 48 hours at 37°C. We used a maximum dose of 1.11 µmol/L for ponatinib, 33a, 36a, and nilotinib. At this point, the luminescence was recorded by following the manufacturer's protocol. The cell viability for each drug-treated condition was calculated relative to no compound treatment (baseline control).

Phenotypic screening of vasculogenesis in HMVEC-Cs

We performed the vasculogenesis assay on HMVEC-Cs to evaluate the toxicity of all tested compounds on a capillary-like network formation ability. Three different batches of HMVEC-Cs (a batch was considered as a different expansion of the primary cell line) were seeded on 45 µL of gel surface of Geltrex in 96-well plates (Greiner µClear, #655090, Greiner Bio-One) at 25,000 cells per well in 50 µL supplemented EBMTM-2 Basal Medium. The cells were incubated with the compounds for 6 hours at 37°C. All the compounds were screened in an eight-dose range, three-fold dilution series, with three technical replicates. We used maximum dose of 25 µmol/L for ponatinib, 100 µmol/L for 33a and 36a. DMSO was used as a vehicle for the compounds and the concentration of DMSO corresponded to that used for each compound. After the incubation, HMVEC-Cs were stained with calcein AM Fluorescent Dye (Corning #354216, Thermo Fisher Scientific) 1/200 dilution in 1x Hanks' Balanced Salt Solution media (Gibco #14185052, Thermo Fisher Scientific) for 25 minutes and subsequently imaged without washing the dye on the IC200 Kinetic Imaging Platform (Vala Sciences) with 4× objective. The number of completely formed loops was quantified using ImageJ version 1.53e analyzer. To establish comparisons across different batches, we normalized the baseline of each batch to the dose 0 (no compound) and expressed loop formation as a percentage (%).

Phenotypic screening of hiPSC-CMs

hiPSC-CMs were plated on Geltrex-coated 384-well plates at 25,000 cells per well (Greiner µClear, #655090, Greiner Bio-One) in 40 µL MM supplemented with 10% KOSR. The next day an additional 40 µL of media was added and cells were grown for a minimum of 5 days prior to analysis. Contractility was measured on three separate differentiation batches each of hiPSC-CMs HD.15S1 and hiPSC-CMs HD.273 (biological replicates). The cells were incubated with the compounds for 4 days at 37°C.

All the compounds were screened in an eight-dose range, three-fold dilution series, with four technical replicates. We used maximum dose of 25 µmol/L for ponatinib, 100 µmol/L for 33a and 36a. DMSO was used as a vehicle for the compounds and the concentration of DMSO corresponded to that used for each compound. The day of imaging, the cells were washed five times with FluoroBrite DMEM (Gibco #A1896701, Thermo Fisher Scientific), loaded with tetramethylrhodamine methyl ester (TMRM) dye (Invitrogen #T668, Thermo Fisher

Scientific) for 50 minutes at 37°C, and contractility time series were acquired at frequency of 50 Hz for a duration of 10 seconds on the IC200 Kinetic Imaging Platform (Vala Sciences) with 20× objective. The results were analyzed using custom particle image velocity software. To compare results from different batches and cell lines, we normalized the baseline of each batch to the dose 0 (no compound) and expressed as peak contraction amplitude normalized percentage (%).

ELISA for Troponin-T in hiPSC-CMs culture media

An ELISA for human Troponin-T (TNNT1 ELISA kit; Invitrogen #EHTNNT1, Thermo Fisher Scientific) was performed in the supernatant of culture media from three different batches with three technical replicates of HD.15S1 hiPSC-CMs treated for 4 days with ponatinib (0.58 μmol/L), compounds 33a (2.45 μmol/L), and 36a (2.8 μmol/L). The drug doses used corresponded to 35 times the respective IC₈₀ concentrations for inhibition of BCR-ABL-T3151 (Supplementary Fig. S3). The same ELISA for human Troponin-T was performed in the supernatant of culture media from HD.15S1 hiPSC-CMs treated for 4 days with siRNA to inhibit TAK1, SLK, FGFR1, and FLT3. The ELISA was performed following the manufacturer's directions. The absorbance was measured by a colorimetric microplate reader (absorbance 450 nm).

Kinase inhibition profiling

In vitro inhibition of ABL and ABL-T3151 kinases was assessed by a Z-LYTE biochemical assay (Thermo Fisher Scientific; ponatinib, 33a, 36a) or KINOMEScan (Eurofins Discovery; nilotinib) and results were expressed as K_d.

The full kinase inhibition profiles of ponatinib, 33a, and 36a (Supplementary Table S1) were determined using the KINOMEScan screening platform (Eurofins Discovery) performed at the IC₈₀ doses for inhibition of BCR-ABL. Results in Supplementary Table S1 are expressed as residual activity (% control). From the resulting profiles, a kinases dendrogram for each compound was generated using TREE-spot Interaction Maps online application (Eurofins Discovery). We established the following thresholds to define “nonselective” (i.e., those that are inhibited by both ponatinib and the new analogues) and “selective” (i.e., those that are inhibited by ponatinib but not by 33a and 36a) kinases and might be responsible for ponatinib's cardiotoxic effects: “Nonselective” kinases were defined as those that were inhibited effectively (<5% residual activity) and were also inhibited by 33a and 36a (<35% residual activity) at their IC₈₀ concentrations for inhibiting BCR-ABL. The relaxed threshold for 33a and 36a was intended to call kinases that were only modestly affected by the chemical modifications as “nonselective”. “Selective” kinases were defined as those that were inhibited (<15% residual activity) by ponatinib but retained most of their activity (>55% residual activity) after incubation with 33a or 36a. The threshold for ponatinib (<15% residual activity) was relaxed in this instance to increase the pool of potentially cardiotoxic kinases.

siRNA knockdowns

hiPSC-CMs were plated in 384-well plates and treated with siRNAs (Dharmacon) at 10 nmol/L concentration with 0.1 μL Lipofectamine RNAiMax (Invitrogen) per well mixed in Opti-MEM (Gibco) transfection media for 4 days. We used the siRNAs (Dharmacon) against the following kinases: HPK1 (GAUACAAUGAGCUGUGUGA, CAA-CAACGUUCUCAUGUCU, GGAGUUAUCUCUGGUUGCA, GAAAGGACCCUCCAUGGG, L-003586-00, # 11184), CDKL2 (GGACUGAGACUAUACCAAU, CGAGAAAUCAAGUUACUAA, GGCCAUUGGUUGUCUGGUA, GAUGAAGUGUAGGAAUAAA,

L-004797-00, # 8999), PCTK2 (GUACAUUAUGCAACAGUAUA, ACAGAUAAAUCUUGACUU, AAUGGAAGCAGAUUAGUA, GGUAUUGCAUCGAGACUUG, L-004835-00, # 5128)), ABL1 (UCACUGAGUUCAGACCUA, AGAUAAACACUCUAAAGCAUA, AAGGGAGGGUGUACCAUUA, CAACAAGCCCACUGUCUAU, L-003100-00, #25), JAK3 (CCUCAUCUCUUCAGACUUA, GCA-GACACUAGCUUGGAA, CGUCCUGGCUCUUAUGUUC, UGUACGAGCUCUUCACCUA, L-003147-00, # 3718), FLT3 (CAA-GAAACGACACCGGAUA, GAAUUUAAGUCGUGUGUUC, GCAAUGAUUUUGGGACUA, CGCAACAGCUUAUGGAAUU, L-003137-00, # 2322), FGFR1 (GCCACACUCUGCACCGCUA, CCACAGAAUUGGAGGCUAC, CAAUUGCCUUCAGUGGG, GAAAUUGCAUCGAGUGCCG, L-003131-00, # 2260), TAK1 (GGCAUUGCUUCUACAAAU, GAGUGAAUCUGGACG-UUUA, GGAAAGCGUUUAUUGUAGA, GCAAUGAGUUGGUUUUAC, L-003790-00, # 6885) SLK (GGUAGAGAUUGA-CAUAUUA, GAAAAGAGCUCAUGAAACG, GCUCGAAGAA-CGACACUUA, GGAACAUAGCCAAGAAUUA, L-003850-00, # 9748), and an internally produced negative control consisting of 48 nontargeting siRNAs in order to dilute any possible off target effects.

For the Troponin-T determinations, hiPSC-CMs were plated in six-well plates and treated with siRNAs (Thermo Fisher Scientific) at 10 nmol/L concentration with 0.1 μL Lipofectamine RNAiMax (Invitrogen) per well mixed in Opti-MEM (Gibco) transfection media for 4 days. We used the siRNAs (Thermo Fisher Scientific) against the following kinases: ABL1 (assay ID: s865), FLT3 (assay ID: s5291), FGFR1 (assay ID: s5164), TAK1 (assay ID: s13766), SLK (assay ID: s18813), and select negative control (Thermo Fisher Scientific # 4390843).

For the CML cell viability assay, K562-WT and K562-T3151 cells were plated in 384-well plate in suspension and treated with siRNAs (Thermo Fisher Scientific) at 20 nmol/L concentration with 0.1 μL Lipofectamine RNAiMax (Invitrogen) per well mixed in Opti-MEM (Gibco) transfection media for 3 days. We used the same siRNAs (Thermo Fisher Scientific) as described above.

Mouse studies

All the *in vivo* studies were approved by Stanford University's Institutional Animal Care and Use Committee [IACUC; Administrative Panel on Laboratory Animal Care (APLAC) number: 32766]. Animal studies were performed according to Federal and State regulations governing the humane care and use of laboratory animals, including the USDA Animal Welfare Act and the Stanford University Assurance of Compliance with Public Health Service Policy on Humane Care and Use of Laboratory Animals. All procedures were performed following the American Veterinary Medical Association Guidelines for the Euthanasia of Animals. The animal care program at Stanford is accredited by Association for Assessment and Accreditation of Laboratory Animal Care International.

Compound formulation and oral gavage

Ponatinib, 33a, 36a, and vehicle (compound formulation) were administered by oral gavage at final volume of 50 μL per mice for each administration. All the animal studies were performed using the same compound formulation with 5% of the volume with DMSO (MPbio, catalog no. 196055) and diluted in 25:70 (%:%) Polyethylene glycol (PEG300, Acros Organics, catalog no. 19222010) (PEG):olive oil (Kirkland Signature Pure Olive Oil). The vehicle control was 5% DMSO, 25% PEG and 70% olive oil. All compounds were formulated just prior to oral administration by

solubilizing the compounds. Individual doses were preheated for 5 minutes at 37°C and vortexed for 15 seconds before administration to ensure a clear homogenous aspect of the solutions. The oral gavage was performed under anesthesia with isoflurane USP (Vet one, Fluriso, NDC 1398504660). The mice were placed in anesthesia induction chambers for approximately 5 minutes until the mice were completely anesthetized using approximately 1.5% isoflurane concentration and 0.5 L per minute oxygen flow rate. The compound administration was performed with 1 mL insulin syringes (Becton Dickinson) with plastic feeding tubes (18 ga × 30 mm; FPT-18-30-50, Instech Laboratories, Inc.).

Pharmacokinetic studies

The pharmacokinetic (PK) studies of ponatinib, 33a, and 36a were conducted as described (25). In brief, 66 C57Bl/6 male mice (purchased from the Jackson Laboratory, stock no. 000664) of 9 to 10 weeks of age were randomized into three groups to be treated with ponatinib ($n = 3/\text{time point}$), 36a ($n = 3/\text{time point}$), and 33a ($n = 3/\text{time point}$) and vehicle ($n = 3$) by oral gavage per each time point: 0, 5, 15, 30, 60, 120, 360 minutes. The animals were treated once with 10 mg/kg by oral gavage for each compound. Blood samples were collected retro-orbitally to analyze the level of compound in blood plasma. Blood plasma was separated via centrifugation at 7,000 RPM for 10 minutes. A 5- μL plasma was taken from each sample and mixed with 995 μL of LC/MS grade acetonitrile that contains 10 ng/mL of internal standard (IS) then vortexed for 30 seconds followed by a 5-minute incubation at room temperature. Mixture was centrifuged at 11,000 RPM for 15 minutes at 4°C and supernatant was collected and further cleaned by recentrifugation. Each protein-free plasma fraction ($n = 3/\text{time point}$) was used to determine the concentration of ponatinib using the high performance liquid chromatography/mass spectrometry multiple reaction monitoring (MRM) method as follows; ponatinib: ponatinib plasma concentration was determined by mass quantification analysis using an Agilent 6490 iFunnl triple quadrupole (QQQ) mass spectrometer equipped with an Agilent 1290 infinity II UHPLC. An Agilent analytical C18 column, ZORBAX C18 (Eclipse Plus C18 reverse phase, 2.1 × 50 mm, 1.8 μm particle size) was used. The mobile phase was composed of 30% water buffered with 0.1% formic acid and 70% acetonitrile buffered with 0.1% formic acid. The flow rate of mobile phase was set at 0.6 mL per minute and column temperature was adjusted at 30°C. The electrospray ionization source was operated in positive ion mode. Mass spectrometer parameters were optimized as: source temperature 550°C, nebulizer gas (nitrogen) 20 psi, IS voltage 5000 V, collision energy 21 V. MRM method was used for the detection of ponatinib and an IS, 3-(Imidazo[1,2-b]pyridazine-3-ylethynyl)-4-methoxy-N-(4-((4-methylpiperazin-1-yl)methyl)-3-(trifluoromethyl) phenyl)benzamide, a similar analogue of ponatinib. The precursor ion $[M+H]^+$ and product ion for ponatinib were monitored at m/z 533.2 and m/z 260.1, respectively. And the precursor ion $[M+H]^+$ and product ion for IS were monitored at m/z 549.3 and m/z 276.2, respectively. A calibration curve was generated using known concentrations of ponatinib and IS, and this curve was used to calculate unknown concentrations of ponatinib in the plasma at different time points.

The PK study for 36a was similar procedure to that described for ponatinib, except the mobile phase, collision energies, and internal standards. The mobile phase was composed of 20% water buffered with 0.1% formic acid and 80% acetonitrile buffered with 0.1% formic acid. Collision energies of 39 V and 46 V were used for 36a and IS, 3-(Imidazo[1,2-b]pyridazine-3-ylethynyl)-N-(3-(4-methyl-1H-imidazol-1-yl)-5-(trifluoromethyl)phenyl)benzamide, a similar analogue of

36a, respectively. The precursor ion $[M+H]^+$ and product ion for 36a were monitored at m/z 501.3 and m/z 260.1, respectively. And the precursor ion $[M+H]^+$ and product ion for IS were monitored at m/z 487.2 and m/z 217.9, respectively.

The PK study for 33a was similar procedure to that described for ponatinib, except the mobile phase, collision energies, and internal standards. The mobile phase and internal standards were same as that used for 36a. Collision energies of 40 V and 46 V were used for 33a and IS, respectively. The precursor ion $[M+H]^+$ and product ion for 33a were monitored at m/z 487.2 and m/z 231.9, respectively.

Toxicity studies

C57Bl/6 male mice of 9 to 10 weeks of age were randomized into four groups to be treated with ponatinib ($n = 5$), 33a ($n = 5$), 36a ($n = 5$), and vehicle ($n = 5$) by oral gavage. The animals were treated with 10 mg/kg by oral gavage for each compound for 5 days and with dose escalation (10 mg/kg) every 5 days reaching 60 mg/kg as the maximum dose (30 days total treatment). After 30 days of treatment all mice were euthanized by CO₂ inhalation for 5 minutes in an optimal CO₂ flow rate (30% to 70% of the chamber or cage volume/min) to minimize animal distress and followed by cervical dislocation as a secondary method of euthanasia.

Human CML xenograft model

9 to 10 weeks old NOD/SCID gamma (NSG) female mice (animals were bred in the Stanford animal facilities) were implanted with 1 million of K562-T135I mutant CML cells in 0.1 mL of Matrigel (Corning #354234; 1:1) subcutaneously into the in right posterior dorsal flank of each mouse. 4 days after the injection, the mice were randomized into four groups ($n = 9$) that received ponatinib, 33a, and 36a (30 mg/kg) and vehicle daily by oral gavage (see methods for compound formulation and oral gavage above). After 3 weeks of treatment, blood samples were collected retro-orbitally from anesthetized mice (~4% isoflurane in oxygen) and all the anesthetized mice were euthanized by cervical dislocation, and tumor, blood, heart, and other organs were collected. This timepoint was selected because control animals were experiencing near maximal allowable tumor burden (as per Stanford IACUC) and significant weight loss. Blood samples were collected for posterior Troponin-I serum level analysis using Siemens Dimension Xpand analyzer and the tumor were explanted for posterior measurements. To determine tumor volume by external caliper, we measure the long diameter ($L1$) and the short diameter ($L2$). Tumor volume was calculated by the formula: tumor volume = $0.5236 \times L1 \times (L2)^2$.

Quantification and statistical analysis

Data are presented as mean \pm SEM as indicated. Statistical analysis was conducted using GraphPad Prism version 9.1.0. Kruskal–Wallis test was used to estimate significance for nonparametric group, and Benjamini–Krieger–Yekutieli two-stage step-up method with 0.05 false discovery rate and Dunn multiple comparison test were used to determine the differences among the groups. Two-way ANOVA was used to estimate significance in parametric groups, and Dunnett test was used to determine differences for multiple comparisons. Survival curves up to 30 days were estimated using Kaplan–Meier analysis, and the log-rank (Mantel–Cox) test was used to estimate the differences among the groups. Dose-response fitting curve were estimated using $\log_{(\text{inhibitor})}$ versus response model with standard slope (Hill-slope = -1). A $P < 0.05$ was considered statistically significant.

Data availability

The data generated in this study are available within the article and its supplementary data files.

Results**Development of new analogue BCR-ABL kinases inhibitors**

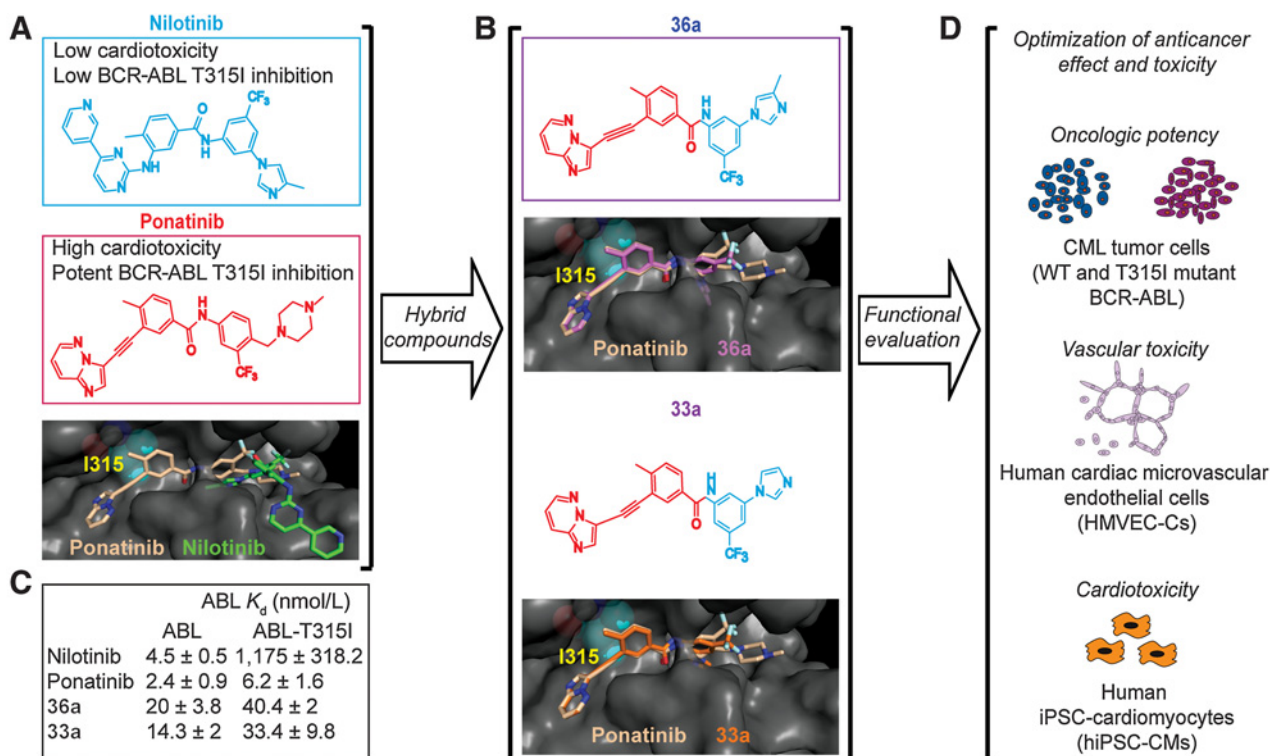
When threonine₃₁₅ is mutated to isoleucine (T315I), the bulkier isoleucine side chain extends into the enzyme active site and prevents entry of nilotinib (as well as the first- and other second-generation BCR-ABL inhibitors; **Fig. 1A**). The third-generation inhibitor ponatinib, however, can enter the active site. Given that nilotinib has a safer cardiotoxicity profile than does ponatinib (26, 27), we hypothesized that it should be possible to create a safer analogue by modifying the structure of ponatinib by incorporating fragments of nilotinib. We generated hybrid compounds 33a and 36a that were predicted to enter the active site and experimentally shown to bind BCR-ABL with high affinity (**Fig. 1B and C**). The chemical syntheses and structure activity relationships of hybrid compounds are described in a companion paper (28). Here, we evaluated these lead compounds and the parent ponatinib in assays for anti-CML proliferation and viability using both WT and T315I mutant BCR-ABL as well as vascular and cardiomyocyte toxicities (**Fig. 1D**).

New ponatinib analogues potently inhibited growth of BCR-ABL-T315I CML cells *in vitro*

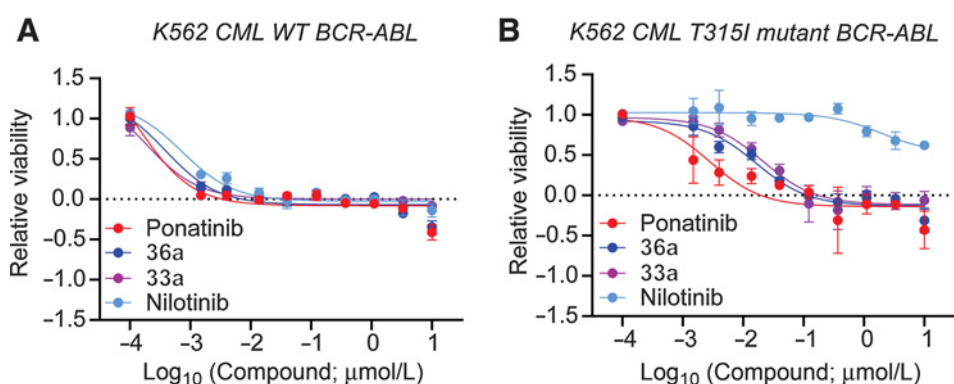
The BCR-ABL-T315I CML *in vitro* model was generated by introducing the “gatekeeper” BCR-ABL T315I mutation using CRISPR in

K562-WT cells (CCL-243 ATCC). A polyclonal T315I mutant K562 cells were enriched by low dose exposure to imatinib (1 $\mu\text{mol/L}$) for 4 weeks and verified by sequencing (Supplementary Fig. S2). Dose-dependent effects on CML viability (expressed as GI_{50}) were measured using the NCI60 methodology (24) following 48 hours of treatment with ponatinib, nilotinib, 33a, and 36a (see Materials and Methods). K562-WT cells (indicating WT BCR-ABL kinase) were susceptible to all compounds, whereas the K562-T315I (indicating the T315I mutated kinase) cells were susceptible to ponatinib, 33a, and 36a but resistant to nilotinib [ponatinib, $\text{GI}_{50} \sim 0.15 \text{ nmol/L}$ (K562-WT) and $\sim 2.79 \text{ nmol/L}$ (K562-T315I); 33a, $\text{GI}_{50} \sim 0.18 \text{ nmol/L}$ (K562-WT) and $\sim 21.06 \text{ nmol/L}$ (K562-T315I); 36a, $\text{GI}_{50} \sim 0.38 \text{ nmol/L}$ (K562-WT) and $\sim 16.48 \text{ nmol/L}$ (K562-T315I); nilotinib $\text{GI}_{50} \sim 0.71 \text{ nmol/L}$ (K562-WT) and 1942 nmol/L (K562-T315I)] (**Fig. 2A and B; Table 1**). The new analogues retained full efficacy against T315I mutated BCR-ABL, albeit with approximately 6.7 times decreased potency compared with ponatinib.

The efficacy of the compounds against the T315I mutant BCR-ABL was tested in another two cell lines: a human CML cell line (KCL22-WT and KCL22-T315I cells; ref. 21) and a murine pro-B cell line (BaF3-WT and BaF3-T315I; ref. 22) for which sublines carry either WT or T315I mutant BCR-ABL genes. The cell lines were treated for 48 hours with ponatinib, nilotinib, 33a, and 36a following the same dose–response experimental design as described above (and in Materials and Methods). The KCL22-WT and BaF3-WT cells showed similar susceptibility to all the compounds,

**Figure 1.**

Development and characterization of the ponatinib analogues. **A**, Chemical structures and molecular docking model of ponatinib and nilotinib to T315I mutant BCR-ABL. **B**, Chemical structures of the hybrid compounds 33a and 36a and molecular docking models showing entry into the binding pocket of T315I mutant BCR-ABL relative to that of ponatinib. **C**, K_d values of the compounds determined for WT and T315I mutant ABL. **D**, Schematic of the *in vitro* bioassays used to characterize the activities of the compounds.

**Figure 2.**

CML *in vitro* antiproliferative activity. Proliferation of CML (K562) cells carrying either WT (A) or CRISPR/Cas9 engineered T315I mutant (B) *BCR-ABL* oncogenes. Data points represent three biological replicates, with four technical replicates per dose in each biological replicate. GI_{50} values are indicated in Table 1.

whereas the KCL22-T315I and BaF3-T315I cells were susceptible to ponatinib, 33a, and 36a but resistant to nilotinib (Supplementary Fig. S3). The new analogues had reproducible efficacy against the T315I mutated *BCR-ABL* across these cell lines.

Compound 33a showed the safest vasculogenesis profile

Direct damage to vascular endothelial cells has been reported to contribute ponatinib-induced vascular adverse events, including occlusive disease (29, 30). We measured vascular toxicity based on the inhibition of vascular networks formed from human microvascular endothelial cells (HMVEC-Cs, Lonza Bioscience; see Materials and Methods; Fig. 3A; ref. 31). Three different batches (biological repli-

cates) of HMVEC-Cs were plated on solidified Geltrex surface in 96-well plate format and treated for 6 hours with eight doses [three-fold dilution series; three technical repeats per dose with ponatinib, 33a, and 36a (maximal doses were 25 $\mu\text{mol/L}$, 100 $\mu\text{mol/L}$, and 100 $\mu\text{mol/L}$, respectively) along with DMSO vehicle control. To establish comparisons across different batches, the baseline of each batch was normalized to the dose 0 (no compound).

33a presented the safest vascular profile ($IC_{50} \sim 22.8 \mu\text{mol/L}$), followed by 36a ($IC_{50} \sim 2.5 \mu\text{mol/L}$). Ponatinib presented the lowest safety ($IC_{50} \sim 0.2 \mu\text{mol/L}$), which is close to its reported free plasma concentration at its clinically used therapeutic dose ($C_{\text{max}} \sim 0.145 \mu\text{mol/L}$; Fig. 3B and C; Table 1; Supplementary Fig. S4; ref. 32).

Table 1. Improvement of 33a and 36a relative to ponatinib.

Compounds	Kinase inhibition and cell viability			
	<i>In vitro</i> ABL inhibition (IC_{50} , nmol/L) mean \pm SEM		K562 cell viability (GI_{50} , nmol/L) mean \pm SEM	
	WT	T315I	WT	T315I
Ponatinib	2.5 \pm 0.3	6.2 \pm 1.1	0.15 \pm 0.2	2.72 \pm 2.0
36a	26.3 \pm 3.8	47.8 \pm 0.2	0.38 \pm 0.2	16.48 \pm 5.0
33a	18.7 \pm 3.5	38.3 \pm 9.5	0.18 \pm 0.1	21.06 \pm 9.0

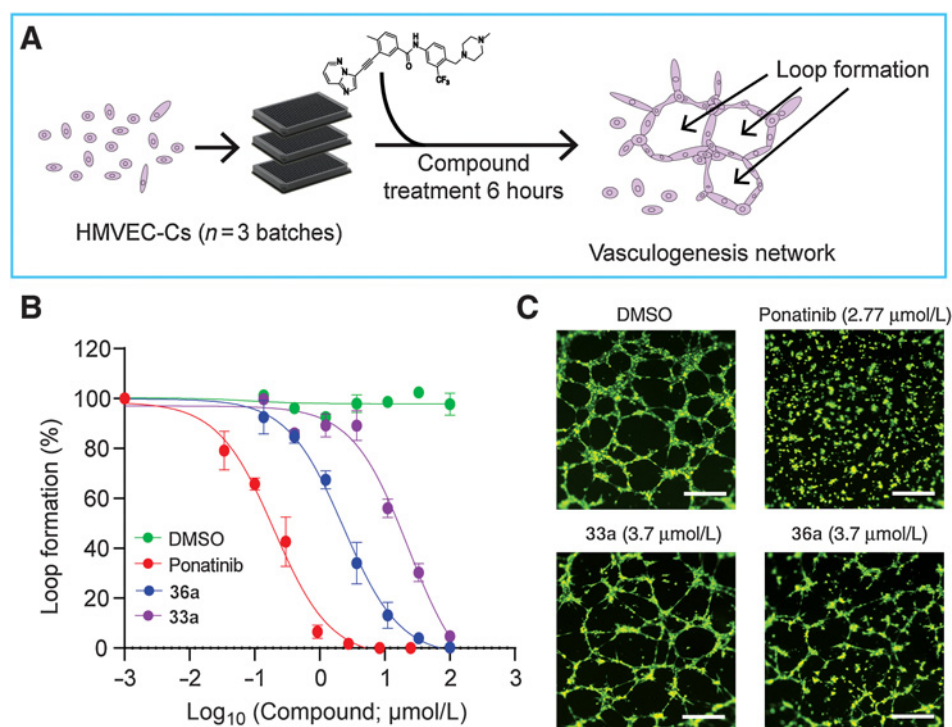
Compounds	Vascular toxicity profile				
	Vasculotoxicity (EC_{50} , $\mu\text{mol/L}$) mean \pm SEM	Ratio tox/ IC_{50}	Improvement ΔEC_{50} tox/ ΔIC_{50} ABL-T315I	Improvement ΔEC_{50} tox/ ΔGI_{50} K562-T315I	Vascular safety ratio IC_{50} compound/ IC_{50} ponatinib
Ponatinib	0.2 \pm 0.04	32.3	1.0	1.0	1.0
36a	2.5 \pm 0.3	52.3	1.6	2.1	12.5
33a	22.8 \pm 4.25	595.3	18.5	15.1	114.0

Compounds	Cardiomyocyte toxicity profile				
	Cardiomyocyte toxicity (EC_{50} , $\mu\text{mol/L}$) mean \pm SEM	Ratio tox/ IC_{50}	Improvement ΔEC_{50} tox/ ΔIC_{50} ABL-T315I	Improvement ΔEC_{50} tox/ ΔGI_{50} K562-T315I	Cardiac safety ratio IC_{50} compound/ IC_{50} ponatinib
Ponatinib	1.5 \pm 0.26	241.9	1.0	1.0	1.0
36a	38.1 \pm 11.63	797.1	3.3	4.3	25.4
33a	>100.0 \pm 0.00	2611.0	>10.8	>8.9	>66.7

Note: Results of kinase inhibition, cell viability, vascular toxicity, and cardiomyocyte toxicity assays. The improvements in vascular and cardiomyocyte toxicity are calculated relative to ponatinib with respect to the potencies of each compound for the inhibition of *in vitro* T315I mutant ABL kinase activity and K562 cell viability. Mean IC_{50} values for vascular toxicity were determined as the mean of three separate experiments (biological replicates), each determined with three technical replicates per dose. Mean IC_{50} values for cardiomyocyte toxicity were determined as the mean from two different donor lines, each determined from three separate experiments (differentiation batches), each of which had four technical replicates per dose. For the *in vitro* ABL inhibition, $n = 2$. Mean GI_{50} values for K562 cell viability were estimated by curve fitting in GraphPad Prism determined from three separate experiments (biological replicates), each determined with four technical replicates per dose (10 doses).

Figure 3.

Effects of 33a and 36a on endothelial cell vasculogenesis. **A**, HMVEC-Cs were treated with compound for 6 hours and the extent of vascular network formation was quantified. **B**, Vascular network loop formation as a function of compound dose. Data points represent averages of three batches from different human donors, three replicates per batch. EC_{50} values are indicated in **Table 1**. **C**, Representative images of vascular networks at the indicated doses. Scale bar, 200 μ m.



33a exhibited an approximately 114 times improved safety margin, followed by 36a that was approximately 12.5 times safer, when compared with ponatinib (**Fig. 3B** and **C**; **Table 1**). Considering the decreased potencies for *in vitro* inhibition of T315I-mutated BCR-ABL, the relative improvements were approximately 18.5 times and approximately 1.6 times for 33a and 36a, respectively. Similarly, considering the GI_{50} potencies, the relative improvements were 15.1 times and 2.1 times for 33a and 36a (**Table 1**), indicating a substantially improved safety margin over ponatinib.

Decreased toxicity of 33a and 36a for hiPSC-CMs contractility

We have shown previously that BCR-ABL and other kinase inhibitor drugs impair hiPSC-CMs contractility, indicating a direct detrimental effect on cardiomyocytes (33). Two different hiPSC-CMs lines were derived from healthy donors: HD.15S1 (male) and HD.273 (female). We studied three differentiation batches for each line (**Fig. 4A**). After passing quality control for differentiation efficiency and cardiomyocyte phenotype (see Materials and Methods), differentiated hiPSC-CMs were metabolically matured for at least for 5 weeks (23). Contractile function was analyzed after 4 days of treatment with ponatinib, 33a, and 36a (maximal doses 25 μ mol/L, 100 μ mol/L, and 100 μ mol/L, respectively) and DMSO (vehicle control) in 384-well plates (eight-dose range response, three-fold change per compound, four technical repeats per dose) determined by a particle image velocity algorithm (see Materials and Methods). Contractile function was expressed as the percentage of the peak contraction amplitude normalized to the baseline of each batch at dose 0 (no compound; **Fig. 4A**) to allow comparisons across different batches and cell lines.

33a presented the safest profile, showing negligible toxicity at the maximal dose tested (IC_{50} > 100 μ mol/L) overlapping values of the DMSO vehicle alone treatment (control; **Fig. 4B** and **C**). 36a presented a safer profile than did ponatinib but nonetheless negatively affected

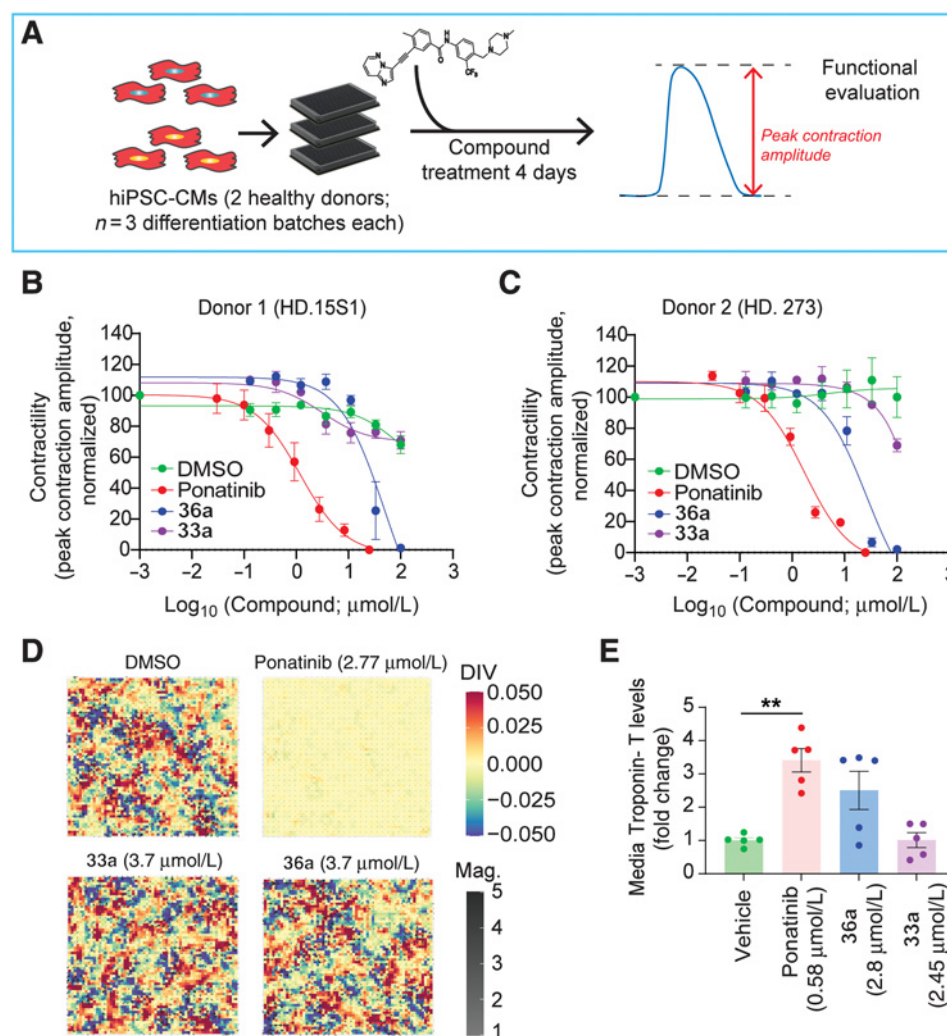
hiPSC-CM contractility (IC_{50} > 38.1 μ mol/L). Ponatinib was the most toxic (IC_{50} > 1.5 μ mol/L; **Fig. 4B** and **C**; **Table 1**). The IC_{50} values represent the mean between the two different cell lines. **Figure 4D** shows representative contraction maps of the treated hiPSC-CMs.

33a and 36a were more than 66.7 times and approximately 25.4 times safer, respectively, than ponatinib in the contractility assay (**Table 1**). Considering the slightly decreased effects on *in vitro* inhibition of T315I mutated BCR-ABL, the net improved safety margin was 10.8 times and 3.3 times for 33a and 36a relative to ponatinib. The numbers were similar considering inhibition of T315I mutated CML: more than 8.9 times and 4.3 times net improvement for 33a and 36a, respectively, relative to ponatinib (**Table 1**). These relative toxicities were similar to those observed for vasculogenesis.

As an independent quantification of myopathic effect, we measured accumulation of cardiac Troponin-T in the hiPSC-CMs culture media from five different batches of HD.15S1 hiPSC-CMs by ELISA (Thermo Fisher Scientific) following 4 days treatment (**Fig. 4E**). The concentration of each compound corresponded to 35 times its IC_{80} for BCR-ABL-T315I (Supplementary Fig. S5). Ponatinib (0.58 μ mol/L) induced substantial cardiac Troponin-T release at whereas 33a (2.45 μ mol/L) did not cause measurable release of cardiac Troponin-T [identical to that of DMSO vehicle (control)]. 36a (2.84 μ mol/L) caused some cardiac Troponin-T release. In summary, ponatinib and 36a caused a myopathic effect at lower doses than impaired contractility while 33a had no measurable direct myopathic effect.

Differential kinase inhibition revealed candidate cardiotoxicity mechanisms

467 total kinases were analyzed by an active site-directed competition binding assay to quantitatively measure differential regulation by 33a, 36a and ponatinib (KINOMEscan, Eurofins Discovery). Each compound was screened at its IC_{80} for *in vitro* inhibition of the ABL-T315I kinase to identify other kinases that are inhibited at

**Figure 4.**

Effects of 36a and 33a on human cardiomyocyte contractility. **A**, hiPSC-CMs were treated with compounds for 4 days and quantitative effects on contractility were measured by optical recording (100 frames/second) and analysis of motion. **B** and **C**, Peak contraction amplitude in response to compound treatment normalized to baseline in cardiomyocytes derived from two healthy donor hiPSC lines. Data points represent averages of three differentiation batches, four replicates per batch. EC_{50} values are indicated in **Table 1**. **D**, Heatmap representations of the peak contraction amplitude in the field of view at the indicated doses. **E**, Troponin-T levels in the media of treated cells analyzed by ELISA. Data points represent biological replicates ($n = 5$), each of which contained three technical replicates. **, $P < 0.01$.

concentrations of inhibitor that block BCR-ABL-T315I (Supplementary Fig. S5). The dendrograms (**Fig. 5A**) represent the kinases that were inhibited beneath a threshold of 35% residual activity (see Materials and Methods). The kinase profiles were broadly similar. Several mutant ABL kinases, in addition to T315I, were inhibited by all three compounds. Also, among the nonselectively inhibited kinases was FLT3, which had been associated with ponatinib-induced cardiotoxicity (29, 30) (% residual activity 1.3, 6.8, 17, for ponatinib, 33a, and 36a, respectively; Supplementary Table S1).

To identify potential mediators of ponatinib cardiotoxicity, we classified kinases that were selectively inhibited by ponatinib (<15% residual activity) but not by 33a and 36a (>55% residual activity), yielding seven kinases: CDKL2, TAK1, FGFR1, SLK, PTCK2 (alternative name CDK17), HPK1 (alternative name MAP4K1), and JAK3 (**Fig. 5B**). Each of these kinases was inhibited by siRNA for 4 days. Relative to negative control siRNA, siRNA knockdown of SLK, TAK1, FGFR1, and FLT3 significantly decreased contractility (22%, 16.5%, 16%, and 14.7%, respectively; **Fig. 5C**). Moreover, inhibition of TAK1 by siRNA induced cardiac Troponin-T release in hiPSC-CMs by approximately 100% relative to control (Supplementary Fig. S6). Thus, the use of 33a and 36a as chemical probes suggested that inhibition of these kinases mediate ponatinib-induced cardiotoxicity.

Finally, we asked if inhibition of these kinases affect CML viability (**Fig. 5D** and **E**). siRNA knockdown of ABL decreased viability of the K-562 CML line carrying either WT or T315I mutant BCR-ABL (to 67% and 63%, respectively of control levels). In contrast, knockdown of SLK, TAK1, FGFR1, and FLT3 had no effect, suggesting that these kinases, at least individually, are not essential to suppress tumor cell growth.

33a and 36a decreased CML tumor burden without cardiotoxicity

To determine the PK of the refined analogues, we administered single oral doses (10 mg/kg) of ponatinib, 33a and 36a to healthy C57BL/6J male mice ($n = 3$ mice/time point per group of treatment) and monitored plasma levels for 360 minutes (**Fig. 6A**). The C_{max} of 33a was 11.5 times higher than ponatinib (2.3 $\mu\text{g/mL}$ versus 0.2 $\mu\text{g/mL}$, respectively) and the t_{max} and $t_{1/2}$ were both longer (t_{max} , 360 minutes versus 120 minutes; $t_{1/2}$, >6 hours versus ~4.5 hours respectively; **Fig. 6B**; Supplementary Fig. S7). 36a presented a higher C_{max} (14.9 $\mu\text{g/mL}$) yet shorter kinetics (t_{max} and $t_{1/2}$ of 30 minutes and ~1 hour, respectively; **Fig. 6B**; Supplementary Fig. S7).

Toxicologic studies (maximum tolerated dose) were performed in 5 healthy C57BL/6J male mice (per group by oral gavage administration

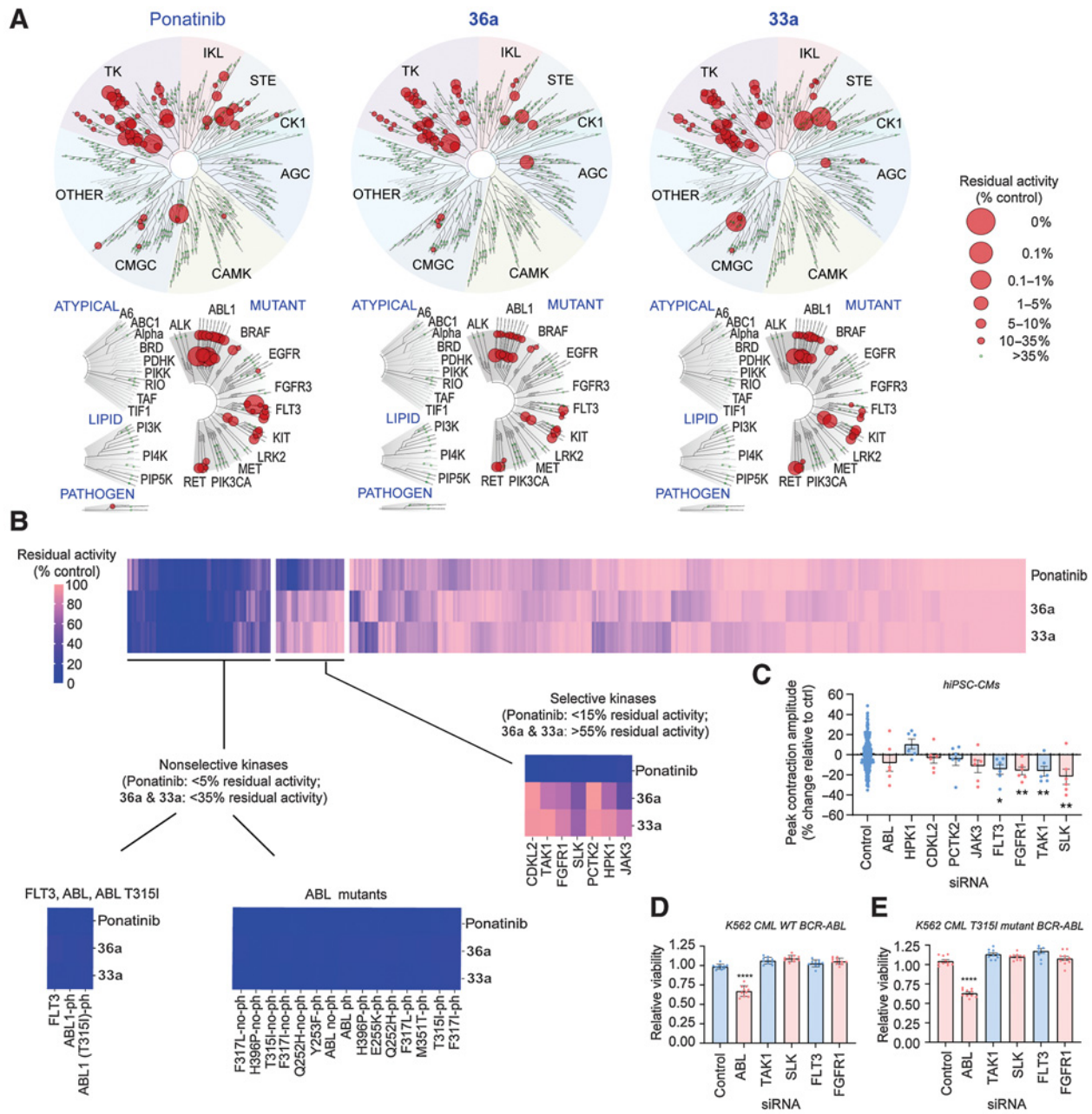


Figure 5. Kinase inhibition profile of 36a and 33a relative to ponatinib. **A**, Dendrogram representation of the kinase inhibition profiles of 33a, 36a, and ponatinib. **B**, Analysis of kinases nonselectively and selectively inhibited by 33a and 36a (relative to ponatinib). Note that all three compounds comparably inhibited mutant ABL kinases. However, a subset of kinases was selectively inhibited by ponatinib. See Supplementary Table S1. **C**, Physiologic effect on human cardiomyocyte contractility (peak contraction amplitude) by individual siRNA knockdown of the kinases that were selectively inhibited by ponatinib, shown relative to the effect of siRNA silencing of ABL. Silencing of most of these kinases degraded contractility, suggesting their potential involvement as mediators of ponatinib cardiotoxicity. **D** and **E**, Effect of siRNA knockdown of the significantly affected kinases in **C** on K562-WT and K562-T315I cell survival. Other than for ABL, knockdowns did not affect cell survival, suggesting that these kinases are not individually essential for tumor growth. *, $P < 0.05$; **, $P < 0.01$; ****, $P < 0.0001$. Ctrl, control.

of ponatinib, 33a, and 36a with a starting daily dose of 10 mg/kg, increasing the dose every 5 days by 10 mg/kg to 60 mg/kg maximum (30 days in total; Fig. 6C). Both 33a and 36a did not cause lethality at the maximal dose (60 mg/kg); however, ponatinib caused lethality at 50 mg/kg (Fig. 6B and D).

A T315I mutant human CML xenograft model was used to evaluate *in vivo* efficacy of 33a and 36a relative to ponatinib (Fig. 6E). K562-T315I cells were implanted subcutaneously into healthy 9- to 10-week-old NSG female mice ($n = 9$ per group of treatment). 4 days after tumor implantation, each group was administered with respective

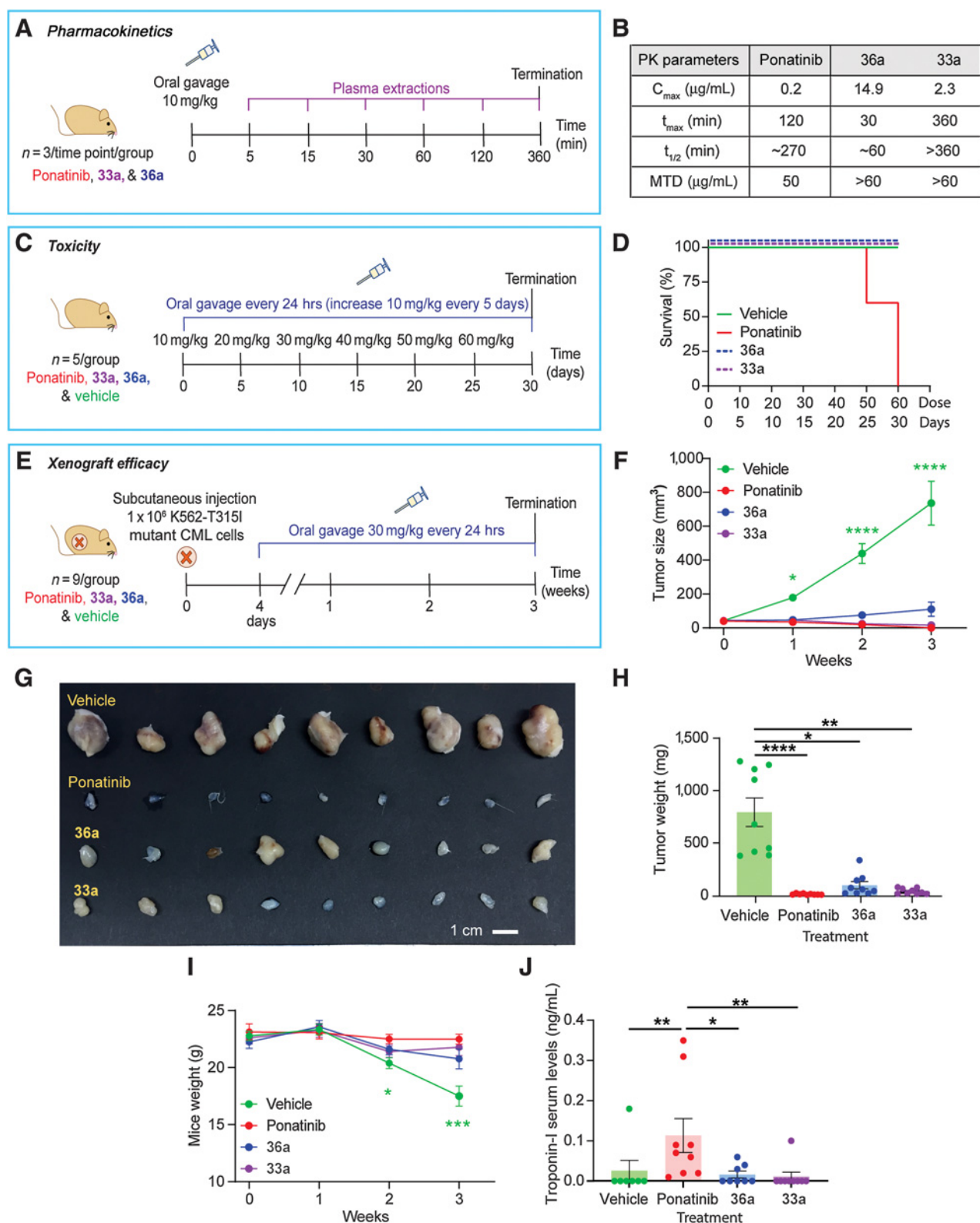


Figure 6.

In vivo assessment of 33a and 36a. **A** and **B**, The PK study design (**A**) and table of resulting parameters (**B**). **C** and **D**, Determination of the maximum tolerated dose (MTD; **C**) and Kaplan–Meier survival curve (**D**). **E**, Xenograft study design. T3151 mutant BCR-ABL K562 cells were implanted in Matrigel plugs and allowed to establish solid tumors for 4 days prior to compound (30 mg/kg) administration by daily oral gavage ($n = 9$ of each group). **F–H**, Tumor size over time (**F**), explanted tumors (**G**), and tumor weights (**H**) at termination (3 weeks). **I**, Body weight of the mice during the study. **J**, Serum Troponin-I levels at termination. *, $P < 0.05$; **, $P < 0.01$; ***, $P < 0.001$; ****, $P < 0.0001$.

compounds (30 mg/kg) by oral gavage daily for 21 days. Both 33a and 36a reduced tumor size relative to treatment with vehicle alone, and with an efficacy statistically indistinguishable from that of ponatinib (Fig. 6F–H). Only the mice with vehicle alone treatment presented significant weight loss (Fig. 6I).

Cardiac serum Troponin-I levels were assessed at the end of the treatment as a biomarker of cardiac damage. Whereas the ponatinib treated mice showed significantly elevated levels of serum cardiac Troponin-I compared with the vehicle alone, the 33a and 36a groups were indistinguishable from the vehicle alone (Fig. 6J).

In summary, 33a and 36a were highly effective against the human K562-T315I CML tumors in the xenograft model yet showed significantly reduced evidence of cardiotoxicity relative to ponatinib. The *in vivo* tumor efficacy and improved safety profile of the refined analogues correlated well with results from the *in vitro* studies.

Discussion

Here we described two refined analogues of ponatinib, 33a and 36a, that retained potency against WT and T315I “gatekeeper” mutant BCR-ABL but had decreased potencies for causing adverse effects on vascular endothelial cell and cardiomyocyte toxicity *in vitro*. Both were efficacious at regression of human BCR-ABL-T315I CML xenografts while 33a showed no evidence of cardiotoxicity.

Ponatinib has the highest risk of cardiotoxicity among BCR-ABL inhibitors. Cardiovascular risks were suggested at the time of approval and became more apparent in the follow up of patients from the PACE (ponatinib Ph-positive acute lymphoblastic leukemia and CML evaluation) clinical trial indicating higher rates of arterial and venous thrombosis than were previously reported (34). Meta-analyses further showed that ponatinib was associated with significant increased risk of cardiovascular occlusive events (35–37). The 2-year follow-up to the phase II PACE trial showed that 17.1% of patients developed arterial occlusive events (AOE), 11.8% of which were classified as serious AOE (38). Moreover, the 5-year follow up showed a cumulative effect of ponatinib toxicity on the occurrence of AOE: 25% AOE (20% serious) in the total population and 31% AOE (26% serious) in the chronic phase of CML due to a longer duration of treatment (34). Strategies to mitigate the risk of cardiovascular events include lower dosing (37, 39, 40) as well as the design of allosteric inhibitors such as asciminib, which has been granted Breakthrough Therapy designation (BTD) by the FDA (41).

Although asciminib is less cardiotoxic than ponatinib, it is ineffective against certain active site ABL mutations that are all inhibited by ponatinib, including F359C, F359I, and F359V, and less effective for F311I and F317 L (42). Furthermore, this same study showed that coadministration with ponatinib increased efficacy against the T315I-mutant kinase and improved survival in mouse xenografts (42). Taken together, ponatinib is likely to remain an important therapeutic for mutant BCR-ABL disease. Although we have not tested our compounds against all known BCR-ABL mutants, they showed similar profile of potencies as ponatinib against all mutants tested (Fig. 5B; Supplementary Table S1) including F317L.

The mechanisms of ponatinib-induced cardiovascular toxicity are not fully understood. Off-target binding of ponatinib to specific kinases is likely to be a major contributor considering that imatinib and the second-generation drugs are safer than ponatinib. In this study, we used compounds 33a and 36a as chemical probes to define kinases that might mediate ponatinib-induced cardiotoxicity. Comparison of the kinase profiles of 33a and 36a with that of ponatinib revealed several novel kinases (SLK, TAK1, FGFR, JAK3, CDKL2, and

PCTK2) that, when tested individually by siRNA knockdown, significantly impaired cardiomyocyte contractility (Fig. 5C). Although ABL and FLT3 also contributed to cardiotoxicity when individually suppressed (Fig. 5C) as seen previously (43, 44), they were comparably inhibited by the refined analogues and the parent ponatinib and hence are unlikely to be responsible for the safer profile of our compounds. Previous studies had associated ponatinib-induced toxicity with inhibition of VEGFR (45), angiotensin receptor TIE-2 (KDR; ref. 46), and the pan-inhibition of all FGFR kinases (47). In addition, TAK1 ablation has been associated with cardiomyocyte death and heart failure in mice (48), and SLK plays roles in modulating apoptosis in ischemia/reperfusion (Mst1 isoform; refs. 49, 50), as well as stress-dependent cardiac hypertrophy and remodeling (Mst2 isoform; ref. 51). Taken together, the use of 33a and 36a as chemical probes of ponatinib-induced cardiotoxicity supported the hypothesis that toxicity was due to off-target effects, and implicated multiple kinases as potential mediators, including SLK, TAK1, JAK3, CDKL2, PCTK2, that had not been previously associated with ponatinib-induced cardiotoxicity.

Finally, 33a and 36a treatment caused regression of human T315I-positive BCR-ABL CML in mouse xenografts, and increased animal survival, with similar efficacies as ponatinib (Fig. 6E and F). In contrast to ponatinib, 33a did not cause accumulation of troponins, which are biomarkers of cardiomyocyte damage, either from hiPSC-CMs treated *in vitro* (Fig. 4E) or in serum of the mouse xenograft models administered the compounds *in vivo* (Fig. 6J).

In conclusion, we engineered analogues of ponatinib with safer cardiovascular toxicity profiles that retained efficacy against CML carrying the T315I “gatekeeper” mutation of BCR-ABL, for which ponatinib is the only approved and effective therapeutic. The approach highlights the potential of realistic human *in vitro* models to reduce the high risk of cardiovascular toxicity that is prevalent among small molecule oncology therapeutics.

Authors' Disclosures

A.P. Hnatiuk reports a patent for “Compounds with improved cardiac safety for the treatment of cancer and neurodegenerative disorders” pending. A.A.N. Bruyneel reports personal fees from McKinsey outside the submitted work; in addition, A.A.N. Bruyneel has a patent for “Compounds with improved cardiac safety for the treatment of cancer and neurodegenerative disorders” pending. M. Pandrala reports a patent for PCT/US22/25400 pending. V. Wiebking reports grants from Deutsche Forschungsgemeinschaft during the conduct of the study and personal fees, nonfinancial support, and other support from Genentech, Inc. outside the submitted work. R. Majeti reports other support from CircBio Inc., Kodikaz Therapeutic Solutions, Pheast Therapeutics, Myelogene; personal fees from Syros Pharmaceuticals; grants and other support from Gilead Sciences; and other support from RNAC Therapeutics outside the submitted work. S.V. Malhotra reports a patent for PCT/US22/25400 pending. M. Mercola reports grants from NIH, European Union Mari Skłodowska-Curie fellowship, other support from Joan and Sanford I. Weill Scholars Endowment, grants from Phospholamban Foundation during the conduct of the study, and personal fees from Vala Sciences, Inc. outside the submitted work; in addition, M. Mercola has a patent for “Compounds with improved cardiac safety for the treatment of cancer and neurodegenerative disorders” pending to Stanford University and Oregon Healthy Sciences University. No disclosures were reported by the other authors.

Authors' Contributions

A.P. Hnatiuk: Conceptualization, formal analysis, validation, investigation, visualization, methodology, writing—original draft, writing—review and editing. A.A. Bruyneel: Conceptualization, formal analysis, validation, investigation, visualization, methodology, writing—original draft, writing—review and editing. D. Tailor: Conceptualization, formal analysis, investigation, visualization, methodology, writing—review and editing. M. Pandrala: Conceptualization, formal analysis, validation, investigation, visualization, methodology, writing—original draft,

writing–review and editing, chemical synthesis. **A. Dheeraj**: Investigation, methodology. **W. Li**: Investigation, methodology. **R. Serrano**: Software, investigation, visualization, methodology. **D.A.M. Feyen**: Software, formal analysis, validation, investigation, visualization, methodology. **M.M. Vu**: Investigation, methodology. **P. Amaty**: Investigation, methodology. **S. Gupta**: Investigation. **Y. Nakauchi**: Investigation, methodology. **I. Morgado**: Investigation. **V. Wiebking**: Methodology. **R. Liao**: Resources, supervision, funding acquisition. **M. Porteus**: Resources, supervision, funding acquisition. **R. Majeti**: Resources, supervision, funding acquisition. **S.V. Malhotra**: Conceptualization, resources, supervision, funding acquisition, project administration. **M. Mercola**: Conceptualization, resources, formal analysis, supervision, funding acquisition, writing–original draft, project administration.

Acknowledgments

This research was supported by grants from the NIH (grant nos. R21GM137151, R01HL152055, R01HL130840, and P01HL141084 to M. Mercola; grant nos. R01DK114174 and R01EY032159 to S.V. Malhotra) and the Joan and

Sanford I. Weill Scholars Endowment (to M. Mercola). D.A.M. Feyen was funded by the European Union's Horizon 2020 research and innovation programme under the Marie Skłodowska-Curie grant agreement no. 708459 and the PLN Foundation. S.V. Malhotra would like to acknowledge the support of the Sheila Edwards-Lienhart Endowment. The graphical abstract was created with www.biorender.com.

The costs of publication of this article were defrayed in part by the payment of page charges. This article must therefore be hereby marked *advertisement* in accordance with 18 U.S.C. Section 1734 solely to indicate this fact.

Note

Supplementary data for this article are available at Cancer Research Online (<http://cancerres.aacrjournals.org/>).

Received October 27, 2021; revised March 29, 2022; accepted May 24, 2022; published first May 31, 2022.

References

- Siegel RL, Miller KD, Jemal A. Cancer statistics, 2020. *CA Cancer J Clin* 2020;70:7–30.
- Mahon FX. Treatment-free remission in CML: who, how, and why? *Hematology Am Soc Hematol Educ Program* 2017;2017:102–9.
- Roskoski R, Jr. Properties of FDA-approved small molecule protein kinase inhibitors: A 2020 update. *Pharmacol Res* 2020;152:104609.
- Jin Y, Xu Z, Yan H, He Q, Yang X, Luo P. A comprehensive review of clinical cardiotoxicity incidence of FDA-approved small-molecule kinase inhibitors. *Front Pharmacol* 2020;11:891.
- Quintas-Cardama A, Cortes JE. Chronic myeloid leukemia: diagnosis and treatment. *Mayo Clin Proc* 2006;81:973–88.
- Mian AA, Oancea C, Zhao Z, Ottmann OG, Ruthardt M. Oligomerization inhibition, combined with allosteric inhibition, abrogates the transformation potential of T3151-positive BCR/ABL. *Leukemia* 2009;23:2242–7.
- Druker BJ, Talpaz M, Resta DJ, Peng B, Buchdunger E, Ford JM, et al. Efficacy and safety of a specific inhibitor of the BCR-ABL tyrosine kinase in chronic myeloid leukemia. *N Engl J Med* 2001;344:1031–7.
- Hehlmann R, Muller MC, Lauseker M, Hanfstein B, Fabarius A, Schreiber A, et al. Deep molecular response is reached by the majority of patients treated with imatinib, predicts survival, and is achieved more quickly by optimized high-dose imatinib: results from the randomized CML-study IV. *J Clin Oncol* 2014;32:415–23.
- Bhamidipati PK, Kantarjian H, Cortes J, Cornelison AM, Jabbour E. Management of imatinib-resistant patients with chronic myeloid leukemia. *Ther Adv Hematol* 2013;4:103–17.
- Bixby D, Talpaz M. Mechanisms of resistance to tyrosine kinase inhibitors in chronic myeloid leukemia and recent therapeutic strategies to overcome resistance. *Hematology Am Soc Hematol Educ Program* 2009;461–76.
- Hochhaus A, O'Brien SG, Guilhot F, Druker BJ, Branford S, Foroni L, et al. Six-year follow-up of patients receiving imatinib for the first-line treatment of chronic myeloid leukemia. *Leukemia* 2009;23:1054–61.
- Deremer DL, Ustun C, Natarajan K. Nilotinib: a second-generation tyrosine kinase inhibitor for the treatment of chronic myelogenous leukemia. *Clin Ther* 2008;30:1956–75.
- Liu J, Zhang Y, Huang H, Lei X, Tang G, Cao X, et al. Recent advances in Bcr-Abl tyrosine kinase inhibitors for overriding T3151 mutation. *Chem Biol Drug Des* 2021;97:649–64.
- Miller GD, Bruno BJ, Lim CS. Resistant mutations in CML and Ph(+)-ALL - role of ponatinib. *Biologics* 2014;8:243–54.
- U.S. Food and Drug Administration. Iclusig® (Ponatinib) tablets for oral use. Prescribing Information. 2016 Nov. Available from: https://www.accessdata.fda.gov/drugsatfda_docs/label/2016/203469s022lbl.pdf.
- U.S. Food and Drug Administration. 2012 Notifications. Available from: <https://www.fda.gov/drugs/resources-information-approved-drugs/2012-notifications>.
- Najjar M, Suebsuwong C, Ray SS, Thapa RJ, Maki JL, Nogusa S, et al. Structure guided design of potent and selective ponatinib-based hybrid inhibitors for RIPK1. *Cell Rep* 2015;10:1850–60.
- Huang W-SS, W C. An efficient synthesis of nilotinib (AMN107). *Synthesis* 2007;14:2121–4.
- Wen M, Shen C, Wang L, Zhang P, Jin J. An efficient d-glucosamine-based copper catalyst for C–X couplings and its application in the synthesis of nilotinib intermediate. *RSC Adv* 2015;5:1522–8.
- Eadie LN, Saunders VA, Branford S, White DL, Hughes TP. The new allosteric inhibitor asciminib is susceptible to resistance mediated by ABCB1 and ABCG2 overexpression in vitro. *Oncotarget* 2018;9:13423–37.
- Oaxaca DM, Y-R SA, Ross JA, Rodriguez G, Staniswalis JG, Kirken RA. Sensitivity of imatinib-resistant T3151 BCR-ABL CML to a synergistic combination of ponatinib and forskolin treatment. *Tumour Biol* 2016;37:12643–54.
- La Rosee P, Corbin AS, Stoffregen EP, Deininger MW, Druker BJ. Activity of the Bcr-Abl kinase inhibitor PD180970 against clinically relevant Bcr-Abl isoforms that cause resistance to imatinib mesylate (Gleevec, STI571). *Cancer Res* 2002;62:7149–53.
- Feyen DAM, McKeithan WL, Bruyneel AAN, Spiering S, Hormann L, Ulmer B, et al. Metabolic maturation media improve physiological function of human iPSC-derived cardiomyocytes. *Cell Rep* 2020;32:107925.
- Shoemaker RH. The NCI60 human tumour cell line anticancer drug screen. *Nat Rev Cancer* 2006;6:813–23.
- Taylor D, Resendez A, Garcia-Marques FJ, Pandrala M, Going CC, Bermudez A, et al. Y box binding protein 1 inhibition as a targeted therapy for ovarian cancer. *Cell Chem Biol* 2021;28:1206–20.
- Francisco ARG, Alves D, David C, Guerra L, Pinto FJ, Almeida AG. Cardiotoxicity in hematological diseases: are the tyrosine kinase inhibitors imatinib and nilotinib safe? *Cardiovasc Toxicol* 2018;18:431–5.
- Singh AP, Umbarkar P, Tousif S, Lal H. Cardiotoxicity of the BCR-ABL1 tyrosine kinase inhibitors: emphasis on ponatinib. *Int J Cardiol* 2020;316:214–21.
- Pandrala M, Bruyneel AAN, Hnatiuk AP, Mercola M, Malhotra SV, et al. Designing novel BCR-ABL inhibitors with improved cardiac-safety. *J. Med. Chem.* 2022. In press.
- Madonna R, Pieragostino D, Cufaro MC, Doria V, Del Boccio P, Deidda M, et al. Ponatinib induces vascular toxicity through the notch-1 signaling pathway. *J Clin Med* 2020;9:820.
- Gover-Proaktor A, Granot G, Pasmanik-Chor M, Pasvolsky O, Shapira S, Raz O, et al. Bosutinib, dasatinib, imatinib, nilotinib, and ponatinib differentially affect the vascular molecular pathways and functionality of human endothelial cells. *Leuk Lymphoma* 2019;60:189–99.
- Stryker ZI, Rajabi M, Davis PJ, Mousa SA. Evaluation of angiogenesis assays. *Biomedicines* 2019;7:37.
- Cortes JE, Kantarjian H, Shah NP, Bixby D, Mauro MJ, Flinn I, et al. Ponatinib in refractory Philadelphia chromosome-positive leukemias. *N Engl J Med* 2012;367:2075–88.

33. Sharma A, BurrIDGE PW, McKeithan WL, Serrano R, Shukla P, Sayed N, et al. High-throughput screening of tyrosine kinase inhibitor cardiotoxicity with human induced pluripotent stem cells. *Sci Transl Med* 2017;9:eaaf2584.
34. Cortes JE, Kim DW, Pinilla-Ibarz J, le Coutre PD, Paquette R, Chuah C, et al. Ponatinib efficacy and safety in Philadelphia chromosome-positive leukemia: final 5-year results of the phase 2 PACE trial. *Blood* 2018;132:393–404.
35. Douxfils J, Haguët H, Mullier F, Chatelain C, Graux C, Dogne JM. Association between BCR-ABL tyrosine kinase inhibitors for chronic myeloid leukemia and cardiovascular events, major molecular response, and overall survival: a systematic review and meta-analysis. *JAMA Oncol* 2016;2:625–32.
36. Casavecchia G, Galderisi M, Novo G, Gravina M, Santoro C, Agricola E, et al. Early diagnosis, clinical management, and follow-up of cardiovascular events with ponatinib. *Heart Fail Rev* 2020;25:447–56.
37. Chan O, Talati C, Isenlumhe L, Shams S, Nodzon L, Fradley M, et al. Side-effects profile and outcomes of ponatinib in the treatment of chronic myeloid leukemia. *Blood Adv* 2020;4:530–8.
38. Cortes JE, Kim DW, Pinilla-Ibarz J, le Coutre P, Paquette R, Chuah C, et al. A phase 2 trial of ponatinib in Philadelphia chromosome-positive leukemias. *N Engl J Med* 2013;369:1783–96.
39. Jabbour E, Short NJ, Ravandi F, Huang X, Daver N, DiNardo CD, et al. Combination of hyper-CVAD with ponatinib as first-line therapy for patients with Philadelphia chromosome-positive acute lymphoblastic leukaemia: long-term follow-up of a single-centre, phase 2 study. *Lancet Haematol* 2018;5:e618–e27.
40. ICLUSIG (ponatinib) tablets. Maximize benefit-risk profile of ICLUSIG in CP-CML with a response-based dosing strategy. Available from: <https://www.iclusig.com/hcp/dosing/recommendations>.
41. Novartis. Novartis receives FDA Breakthrough Therapy designations for investigational STAMP inhibitor asciminib (ABL001) in chronic myeloid leukemia. Basel (Switzerland): Novartis; 2021 Feb 8. Available from: <https://www.novartis.com/news/media-releases/novartis-receives-fda-breakthrough-therapy-designations-investigational-stamp-inhibitor-asciminib-abl001-chronic-myeloid-leukemia>.
42. Eide CA, Zabriskie MS, Savage Stevens SL, Antelope O, Vellore NA, Than H, et al. Combining the allosteric inhibitor asciminib with ponatinib suppresses emergence of and restores efficacy against highly resistant BCR-ABL1 mutants. *Cancer Cell* 2019;36:431–43.
43. Hasinoff BB, Patel D, Wu X. The myocyte-damaging effects of the BCR-ABL1-targeted tyrosine kinase inhibitors increase with potency and decrease with specificity. *Cardiovasc Toxicol* 2017;17:297–306.
44. Grabowska ME, Chun B, Moya R, Saucerman JJ. Computational model of cardiomyocyte apoptosis identifies mechanisms of tyrosine kinase inhibitor-induced cardiotoxicity. *J Mol Cell Cardiol* 2021;155:66–77.
45. Ai N, Chong CM, Chen W, Hu Z, Su H, Chen G, et al. Ponatinib exerts anti-angiogenic effects in the zebrafish and human umbilical vein endothelial cells via blocking VEGFR signaling pathway. *Oncotarget* 2018;9:31958–70.
46. Li X, Cai Y, Goines J, Pastura P, Brichta L, Lane A, et al. Ponatinib combined with rapamycin causes regression of murine venous malformation. *Arterioscler Thromb Vasc Biol* 2019;39:496–512.
47. Gozgit JM, Wong MJ, Moran L, Wardwell S, Moheemad QK, Narasimhan NI, et al. Ponatinib (AP24534), a multitargeted pan-FGFR inhibitor with activity in multiple FGFR-amplified or mutated cancer models. *Mol Cancer Ther* 2012;11:690–9.
48. Li L, Chen Y, Doan J, Murray J, Molkenin JD, Liu Q. Transforming growth factor beta-activated kinase 1 signaling pathway critically regulates myocardial survival and remodeling. *Circulation* 2014;130:2162–72.
49. Odashima M, Usui S, Takagi H, Hong C, Liu J, Yokota M, et al. Inhibition of endogenous Mst1 prevents apoptosis and cardiac dysfunction without affecting cardiac hypertrophy after myocardial infarction. *Circ Res* 2007;100:1344–52.
50. Yamamoto S, Yang G, Zablocki D, Liu J, Hong C, Kim SJ, et al. Activation of Mst1 causes dilated cardiomyopathy by stimulating apoptosis without compensatory ventricular myocyte hypertrophy. *J Clin Invest* 2003;111:1463–74.
51. Zi M, Maqsood A, Prehar S, Mohamed TM, Abou-Leisa R, Robertson A, et al. The mammalian Ste20-like kinase 2 (Mst2) modulates stress-induced cardiac hypertrophy. *J Biol Chem* 2014;289:24275–88.